Journal of ELECTRONIC MATERIALS, Vol. 50, No. 1, 2021
https://doi.org/10.1007/s11664-020-08504-0
© 2020 The Minerals, Metals & Materials Society

Study on Microstructure and Shear Property of Cu/In-*x*Cu/Cu Transient Liquid Phase Bonding Joints

ZHENG LIU,[1] LI YANG ,[1,5] YU HANG XU,[2] YAO CHENG ZHANG,[3] KAI JIAN LU,[2] FENG XU,[3] and HUI MING GAO[4]

1.—School of Mechanical Engineering, Guilin University of Aerospace Technology, Guangxi 541004, People's Republic of China. 2.—School of Mechanical Engineering, Soochow University, Jiangsu 215021, People's Republic of China. 3.—School of Automatic Engineering, Changshu Institute of Technology, Jiangsu 215500, People's Republic of China. 4.—National Dies and Molds Quality Supervision Test Center, Jiangsu 215300, People's Republic of China. 5.—e-mail: linlideyu@126.com

Transient liquid phase (TLP) bonding is a promising interconnection technology for high-temperature electronic packaging. In this paper, the effect of Cu particles on the microstructure and shear property of Cu/In-*x*Cu/Cu TLP joints was investigated. The results show that Cu/In-*x*Cu/Cu joint is mainly composed of an In and $Cu_{11}In_9$ phase after bonded for 60 min. A small amount of Cu_2In phase forms at the interface of Cu/$Cu_{11}In_9$ with bonding time exceeding 300 min. The bonding efficiency and shear property of In-Cu mixed particle solder joint are superior to that of the In foil solder joint, because the bonding time was reduced and the shear strength of the solder joint was improved. The phase composition of $Cu_{11}In_9$ and Cu_2In in the joint increased, the porosity decreased and the shear strength increased with increasing Cu content. When the Cu content of the In-*x*Cu solder was 45 wt.%, the shear strength of the Cu/In-45Cu/Cu joint reached the peak value of 15.7 MPa.

Key words: In-*x*Cu mixed particles, transient liquid phase, microstructure, shear property

INTRODUCTION

The application of power electronic devices operated in harsh environments such as high temperature, strong radiation and large pressure increases with the development of many industries such as aerospace, nuclear, deep oil and gas drilling.[1–4] Wide-bandgap semiconductors, especially represented by SiC and GaN that can be theoretically operated at 600°C, are candidates for high-temperature electronic devices.[5,6] The trend in high-temperature applications brings great challenges to microelectronics technology, and traditional soldering methods have failed to meet the manufacturing requirements of advanced electronic systems.

High-temperature solders, such as Pb-based, Pb-free and nanoparticle solder pastes have been chosen as the die-attach material for high-temperature electronic packaging. Pb-based high-temperature solders (Sn-37Pb and Pb-10Sn-2Ag), or Pb-free solders (Au-based and Bi-based solders) are limited by toxicity to the environment, low mechanical properties, high cost, or poor thermal and electrical conductivities.[7–11] In addition, thermal damage and residual stress to the power devices occur as these high-temperature solders are reflowed at high temperature. Although nano-Ag and nano-Cu paste can be sintered at a low temperature to produce high melting point alloys, high porosity of the joint, poor conductivity and thermal conductivity, and high possibility of electro-migration and the high cost should be further improved.[12–14] Transient liquid phase (TLP) bonding technology is recognized as a promising technology to produce heat-resistant joints that are fully

(Received June 11, 2020; accepted September 21, 2020; published online October 10, 2020)

composed of high melting point intermetallic compounds (IMCs) as a result of the low processing temperature and high operation temperature.[15]

Cu-Sn solder has been widely used in the semiconductor industry due to the low cost, high electronic conductivity and low melting temperature.[16–18] However, some reliability problems of the Cu-Sn bonding system exist on account of the formation of brittle Cu-Sn IMCs and Kirkendall voids.[19–21] Moreover, the melting point of Sn (231°C) is higher than that of In (156°C), and the bonding temperature is relatively high, so it is difficult to use in chip bonding which needs a low-temperature process. The lower melting point of In is not only conducive to packaging at low temperature, but also can greatly reduce the manufacturing cost of solder joint. As a low temperature bonding system, the Cu-In system has a good application prospect. There is some research on this system, mainly focusing on the microstructure of Cu-In IMCs and theoretical analysis of growth kinetics.[16,22–24] However, there are few studies on the microstructure evolution of solder joints under different process parameters, corresponding mechanical properties and electrical properties changes. The melting points of different IMC phases vary greatly, and the IMC phase is a hard brittle phase. In order to improve the high temperature resistance of solder joint, it is necessary to form high melting point IMC phase in the weld. Therefore, it is essential to study the microstructure evolution and shear property of solder joints under different process parameters.

In this study, In-*x*Cu mixed particles solder paste is applied as interlayer to bond Cu–Cu substrates by TLP bonding technology. The effect of Cu content on the microstructure and shear property of joints by varying mass percentage of Cu particles to In particles was investigated.

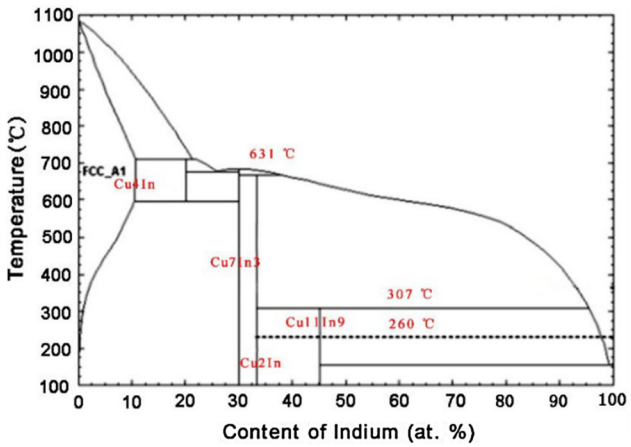

Fig. 1. Phase diagram of Cu-In binary alloy.

EXPERIMENTAL

The phase diagram of Cu-In binary alloys (Fig. 1) shows that Cu_7In_3, Cu_2In and $Cu_{11}In_9$ are stable IMCs at ambient temperature and the melting point of $Cu_{11}In_9$ (307°C) is lower than that of Cu_7In_3 and Cu_2In (up to 631°C). Theoretical calculations are carried out according to the compositions of In-Cu IMC phases ($Cu_{11}In_9$, Cu_2In and Cu_7In_3). The mass percentage of Cu atoms in the In-Cu IMCs (V) is calculated by the following expression:

$$V = nM_{Cu}/(nM_{Cu} + mM_{In}) \quad (1)$$

where M is molar mass, n and m are the number of Cu and In atoms in Cu-In IMCs. The mass percentage of Cu atoms in the In-Cu IMCs is from 40 wt.% to 60 wt.%. Therefore, In-*x*Cu (25, 35, 45 and 55 wt.%) mixed particles are chosen to bond the Cu–Cu substrates.

Pure (99.99 wt.%) In particles (1–8 μm) and pure (99.99 wt.%) Cu particles (1–8 μm) were ultrasonically washed with deionized water and anhydrous alcohol, and then dried. To remove the oxide layer, a 50 μm-thick In layer and upper copper substrate with dimensions of 12 × 12 × 3.95 mm^3 and bottom copper substrate with dimensions of 10 × 10 × 4 mm^3 were cleaned in a 5% HNO_3 solution for 5 min. In-*x*Cu mixed particles were prepared by ultrasonic assisted mixing, and then mixed with 10 wt.% flux to prepare In-*x*Cu mixed particles solder paste. As shown in Fig. 2, the solder paste was printed on the bottom substrate by coating, slipping and drying, and then the upper substrate was placed on the surface to form a sandwiched structure. The height of the homemade mold is 50 μm larger than that of the copper substrate, ensuring that the thickness of the solder paste is 50 μm during the coating. The bonding process was carried out by TWB-100 wafer bonding machine under a vacuum below 5 Pa, as shown in Fig. 3.

Microstructure was characterized by optical microscope (OM, Olympus GX51) and scanning electron microscope (SEM, Supra 55) with an energy dispersive spectroscopy system (EDS, 51-XMX1004). Shear test of the joints was carried out using a UTM5305 electronic universal testing machine with a shear rate of 0.02 mm/min, and fracture morphology of the joints was observed by SEM.

RESULTS AND DISCUSSION

Cu/In/Cu TLP Joints

Figure 4 shows the microstructure of Cu/In/Cu TLP joints bonded at 260°C for 60 min and 300 min under a bonding pressure of 0.1 MPa. The Cu/In/Cu TLP joint consists of an In zone and $Cu_{11}In_9$ phase, and the island-shaped In is wrapped by $Cu_{11}In_9$ at a bonding time of 60 min, as shown in Fig. 4a. Cu atoms rapidly diffuse from the Cu substrate into the

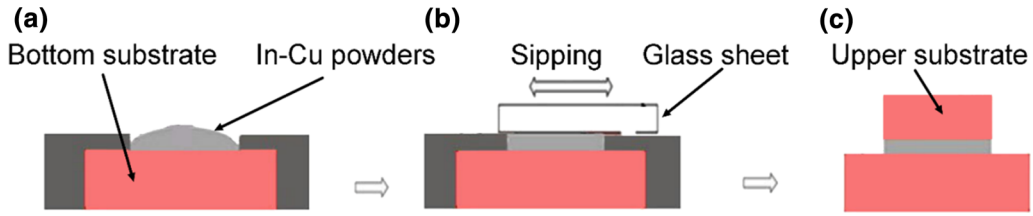

Fig. 2. Schematic of solder paste coating process before bonding.

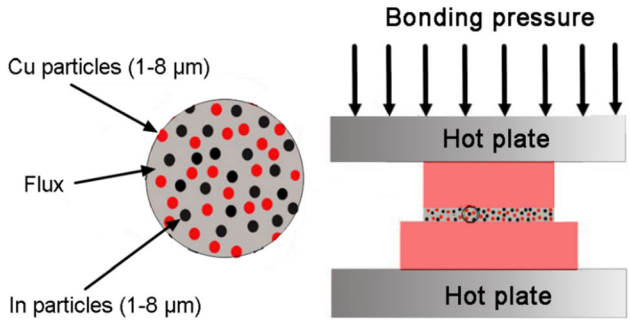

Fig. 3. Schematic diagram of Cu/In-xCu/Cu TLP joints for bonding process.

liquid In after the bonding temperature rose above the melting point of In. When the solubility of Cu in the liquid In reached saturation state at 260°C, $Cu_{11}In_9$ started to precipitate, and the reaction is listed as follows:

$$11Cu + 9In \rightarrow Cu_{11}In_9 \quad (2)$$

$Cu_{11}In_9$ formed at the surface of Cu substrate and gradually grew from the interface of Cu/In toward the center of the joint, and the residual In in the middle of the joint was surrounded by $Cu_{11}In_9$. The TLP joint was mainly composed of Cu_2In and $Cu_{11}In_9$ with bonding time exceeding 300 min, as shown in Fig. 4c. In was completely consumed and Cu_2In layer was formed with a thickness of less than 2 μm along the interface of Cu/$Cu_{11}In_9$, and the following reaction took place.

$$Cu_{11}In_9 + 7Cu \rightarrow 9Cu_2In \quad (3)$$

The growth rate of the $Cu_{11}In_9$ phase at a bonding temperature of 260°C is much higher than that of Cu_2In, indicating that the activation energy of $Cu_{11}In_9$ is smaller than that of Cu_2In. The study developed by Tian[25] showed that the Kirkendall voids formed along the Cu substrate layer in the joint bonded at 260°C for 40 min and gradually grew with prolonging bonding time. Kirkendall voids are barely observed at the interface of Cu/$Cu_{11}In_9$. The initiation and growth of the voids are suppressed as a result of the pressure of 0.1 MPa applied to Cu/In/Cu TLP joints during bonding process.

The shear strength of a Cu/In/Cu TLP joint bonded for 60 min is 6.4 MPa and then increased to 12.3 MPa for the joint bonded for 300 min, indicating that increasing bonding time improved the shear strength of the TLP joint. The residual In of poor mechanical properties within the TLP joint (Fig. 4a) affected the mechanical properties of the joint, resulting in a decrease of the shear strength of the joint. From shear fracture surface of the joints (Fig. 5a), a large number of oblique dimples were observed throughout the fracture surface of the joint bonded for 60 min on account of the superior ductile of In (b). The rock-candy shaped $Cu_{11}In_9$ grain was observed at the fracture face of the joint bonded for 300 min (Fig. 5c), indicating that the fracture mode of the joint is brittle.

The thermal stability and shear strength of Cu_2In are superior than that of $Cu_{11}In_9$, while the slow growth rate of Cu_2In restricts the production of power devices. The growth of Cu_2In was promoted by improving bonding temperature and bonding time.[26,27] The rise of manufacturing cost and thermal damage to temperature-sensitive electronic components was caused by hot-pressing bonding at high temperature for a long time.[28] Therefore, the heat-resistant Cu/In/Cu TLP joints with excellent mechanical properties bonded for 60 min under low temperature is of great significance for the development and application of Cu/In system in the third-generation semiconductor-based power device packaging.

Microstructure of Cu/In-xCu/Cu TLP Joints

Figure 6 shows the microstructure of Cu/In-xCu/Cu (x = 25 wt.%, 35 wt.%, 45 wt.% and 55 wt.%) TLP joints bonded for 60 min at 260°C under a bonding pressure of 3 MPa. As shown in Fig. 6a, Cu/In-25Cu/Cu joint mainly consists of the diffusion reaction zone I ($Cu_{11}In_9$) at the surface of Cu substrate and mixed particles in the *in situ* reaction zone II ($Cu_{11}In_9$ and residual In). Hackly $Cu_{11}In_9$ was formed in zone I, and block shaped $Cu_{11}In_9$ was separated by the residual In in zone II. Cu particles fully participated in the reaction with In and sufficient In reacted with Cu substrate to form a thick $Cu_{11}In_9$ layer in zone I due to the relatively high content of In in the Cu/In-25Cu/Cu TLP joint. The Cu/In-35Cu/Cu TLP joint is mainly composed of $Cu_{11}In_9$. The thickness of zone I and the $Cu_{11}In_9$ phase spacing in zone II increased compared with the Cu/In-25Cu/Cu TLP joint. Sufficient Cu participated in the reaction with In, which caused the

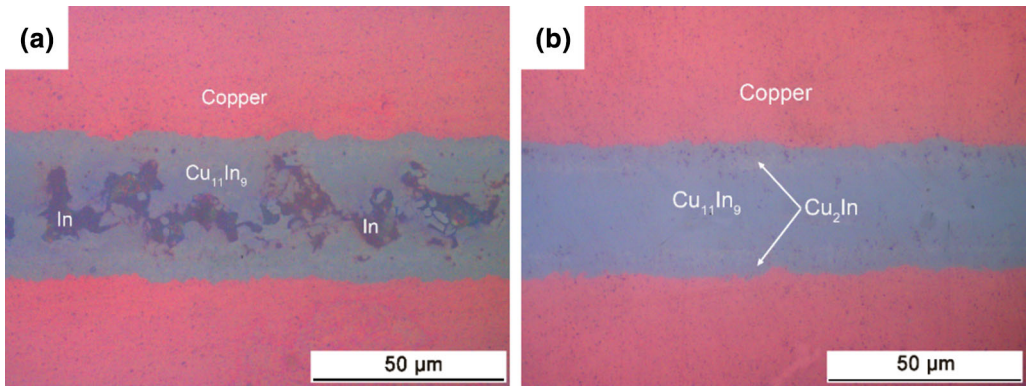

Fig. 4. Microstructure of Cu/In/Cu joints under the bonding temperature of 260°C for (a) 60 min and (b) 300 min.

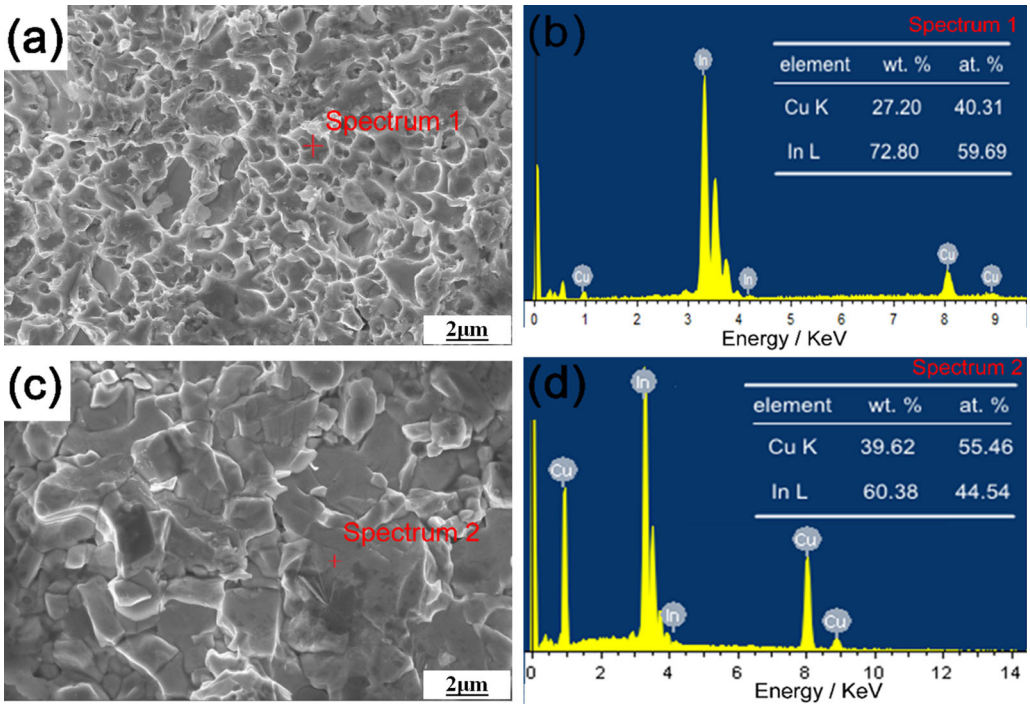

Fig. 5. Fracture surfaces and EDS results of Cu/In/Cu joints with bonding time: (a) 60 min (b) spectrum 1, (c) 300 min and (d) spectrum 2.

increase of $Cu_{11}In_9$ content and decrease of the residual In content in zone II. The In participating in the interfacial reaction with the Cu substrate was reduced by increasing the Cu content. The Cu/In-45Cu/Cu TLP joint is mainly composed of $Cu_{11}In_9$, Cu_2In and a small amount of residual Cu particles. The thickness of the IMC layer in zone I further reduced, and the densest microstructure was obtained among the all Cu containing solder joints.

A large number of residual Cu particles surrounded by Cu_2In are observed in the Cu/In-55Cu/Cu TLP joint, and numerous voids formed among the Cu_2In particles, as shown in Fig. 6d. The gap among the Cu particles cannot be completely filled by In after the flux volatilized because of a small amount of In in the Cu/In-55Cu/Cu TLP joint, resulting in the formation of voids in zone II. Zone I is reduced due to the insufficient In content in Cu/In-55Cu/Cu TLP joint. Thus, the formation of Cu-In IMCs can be promoted by increasing Cu particles content; however, the excess addition of Cu particles leads to the formation of voids, and 45 wt.% of Cu particles addition is acceptable.

Shear Property of Cu/In-*x*Cu/Cu TLP Joints

Figure 7 shows the shear strength of Cu/In-*x*Cu/Cu (x = 25 wt.%, 35 wt.%, 45 wt.%, 55 wt.%) TLP joints bonded for 60 min at 260°C under a bonding pressure of 3 MPa. The shear strength of the joint gradually increased and then reduced with increasing Cu content. The maximum shear strength reaches 15.7 MPa of the solder joint with 45 wt.% Cu content. The shear strength of the TLP joints is

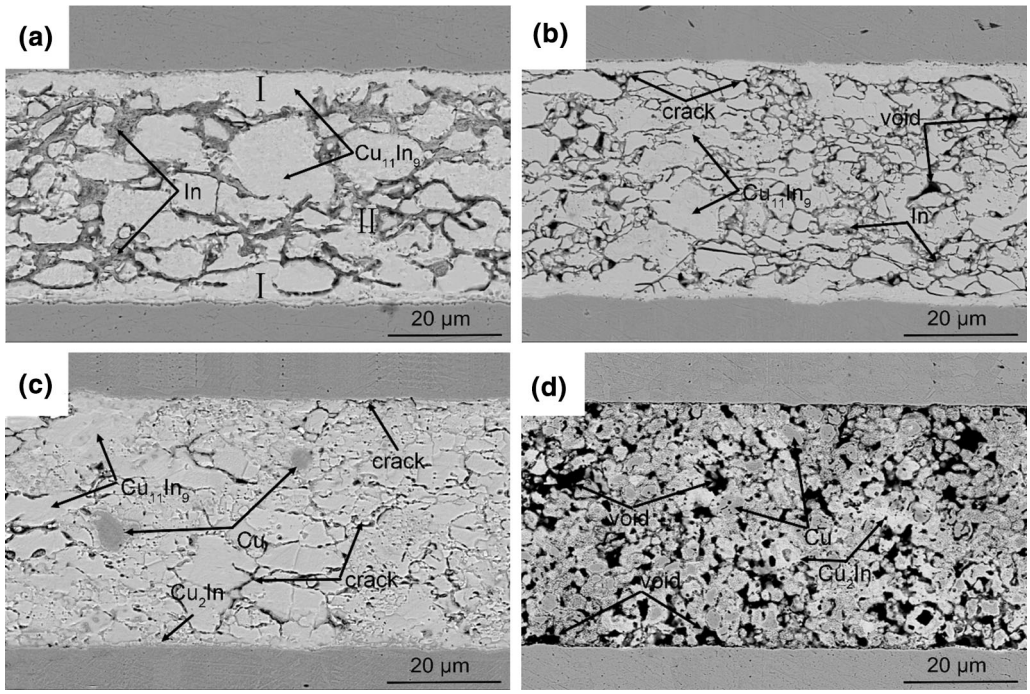

Fig. 6. Microstructure of (a) Cu/In-25Cu/Cu, (b) Cu/In-35Cu/Cu (c) Cu/In-45Cu/Cu and (d) Cu/In-55Cu/Cu TLP joints.

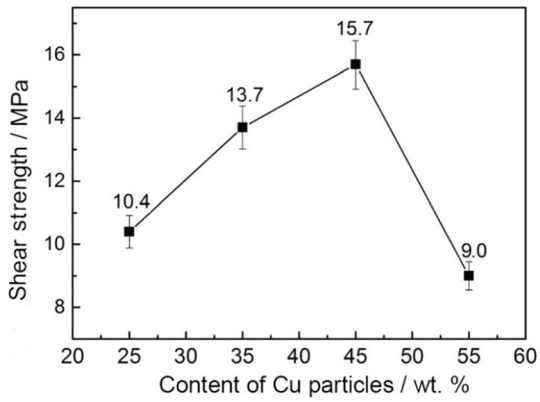

Fig. 7. Shear strength of Cu/In-xCu/Cu (x = 25 wt.%, 35 wt.%, 45 wt.% and 55 wt.%) joints.

controlled by the change of voids and phases transition as a result of the increase of Cu content in the TLP joints. The residual In in the matrix weakens the shear strength of the TLP joints when the Cu content is low (Fig. 6a). The content of high strength phases ($Cu_{11}In_9$, Cu_2In and Cu) in the TLP joints increased and the voids decreased with increasing the Cu content (Fig. 6b–c), resulting in the improvement of shear strength. However, a large number of voids in the *in situ* reaction zone of the joint decreased the shear strength of the joint when Cu content increased to 55 wt.% (Fig. 6d).

Figure 8 shows the shear fracture surface of Cu/In-xCu/Cu (x = 25 wt.%, 35 wt.%, 45 wt.% and 55 wt.%) TLP joints. As shown in Fig. 8a, the IMC phases on the fracture locations were determined to be $Cu_{11}In_9$ by EDS. Shear bands and tearing edge of ruptured In are observed on the surface of the Cu/In-25Cu/Cu TLP joint, indicating a mixed mode of cleavage and plastic fracture. Some defects (pores and micro-voids) are also observed on the surface of the shear fracture. The pores with an irregular shape are among the IMC particles and the inside of the pores are mainly free-grown $Cu_{11}In_9$ grains, and the micro-voids with a regular shape are located inside the IMC particles. The volatilization of flux in the joint resulted in the formation of pores, and these pores allow the IMCs to grow freely during bonding process. The cracks generated from the defects and propagated along the interior of $Cu_{11}In_9$ grain. The fracture surface of Cu/In-35Cu/Cu TLP joint is shown in Fig. 8c. The flat shear bands and a small amount of rock-candy grain facets are found on the fracture surface, indicating that the fracture modes are cleavage fracture and intergranular fracture. The quantity and size of the pores on the fracture surface are reduced with increasing Cu content. The crack nucleated from the pores and micro-voids expanded lager when the joint is subjected to shear stress. When the crack propagated to the grain boundary, the intergranular fracture preferred to occur in the defect areas.

The fracture microstructure of the joint became denser with increasing Cu content to 45 wt.%. A large number of small rock-candy grain facets are observed on the fracture surface, showing that the fracture mode is intergranular. $Cu_{11}In_9$ and Cu_2In in the rock-candy grain facets are detected by EDS, indicating that the phase transformation from $Cu_{11}In_9$ to Cu_2In, which is consistent with the microstructure of the Cu/In-45Cu/Cu TLP joint

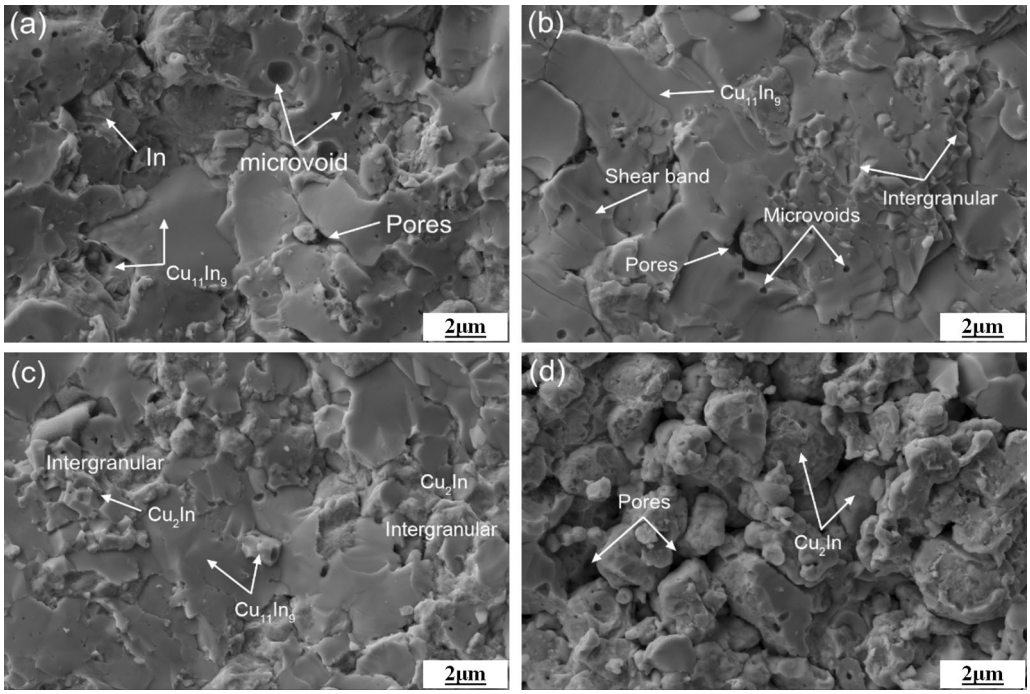

Fig. 8. Fracture surfaces of (a) Cu/In-25Cu/Cu, (b) Cu/In-35Cu/Cu (c) Cu/In-45Cu/Cu and (d) Cu/In-55Cu/Cu joints.

(Fig. 6c). It is supposed that the fracture located at the grain boundaries between $Cu_{11}In_9$ and Cu_2In and the grain boundaries strength between $Cu_{11}In_9$ and Cu_2In is smaller than the intra-granular strength of the two phases. A quantity of free-grown Cu_2In particles and pores in *in situ* reaction zone are observed on the fracture surface of Cu/In-55Cu/Cu TLP joint (Fig. 7d). The pores form along the Cu substrate and form unconnected regions, which significantly reduces the strength of solder joints.

It can be concluded that using In-Cu mixed particles to form Cu/In-*x*Cu IMCs/Cu (x = 25 wt.%, 35 wt.%, 45 wt.%, 55 wt.%) TLP joints significantly improve the shear strength of joints. In addition, the formation rate of the joint is improved by In reacting with the Cu substrate and the Cu particles simultaneously compared with Cu/In/Cu TLP joint. However, pores are easily formed inside the Cu/In-*x*Cu/Cu solder joints and affect the shear property of the joints significantly. Therefore, it is necessary to apply a large bonding pressure (3 MPa) to suppress the formation of voids in the TLP joints.

In this paper, the effect of Cu particles on microstructure and shear property of Cu/In-*x*Cu/Cu TLP joints was investigated. In the future, the microstructure evolution under the action of electromigration and thermal cycle, and the creep property of solder joint can be studied. It is of great significance to further study the reliability of the solder joint.

CONCLUSIONS

1. The Cu/In/Cu TLP joint consisted of In and $Cu_{11}In_9$ phase, and the residual In in the middle of TLP joint is surrounded by $Cu_{11}In_9$ with the bonding time of 60 min. $Cu_{11}In_9$ grew at the expense of In consumption and a small amount of Cu_2In was formed along the interface of Cu/$Cu_{11}In_9$ with the increase of bonding time. The shear strength of the joint is increased by prolonging the bonding time.
2. The bonding time is significantly reduced by *in situ* reaction in addition to interfacial diffusion reaction for Cu/In-*x*Cu/Cu TLP joints. Residual In and cracks exist in the joints with low Cu containing (25 wt.% and 35 wt.%) Cu-In solders and many pores generated with the high Cu containing (55 wt.%) Cu-In solder. The Cu/In-45Cu/Cu TLP joints has the densest microstructure among the all Cu containing solders.
3. Shear strength of Cu/In-*x*Cu/Cu TLP joints firstly increased and then decreased with increasing Cu content. Cu/In-45Cu/Cu TLP joint possesses optimal shear strength of 15.7 MPa among the Cu/In-*x*Cu/Cu TLP joints. The shear strength of the TLP joints is affected by the change of voids and phase transition on account of the increase of Cu content in the TLP joints.

ACKNOWLEDGMENTS

This research was financially supported by the National Natural Science Foundation of China (Foundation No. 51865006) and Natural Science Foundation of the Jiangsu Higher Education Institutions of China (Grant Nos. 19KJA430001 and 18KJA460001).

CONFLICT OF INTEREST

The authors declare that they have no conflict of interest.

REFERENCES

1. K. Sakiko and Y. Takeshi, *JOM* 70, 1 (2018).
2. K. Li, P. Evans, and M. Johnson, *IET Electr. Syst. Transp.* 8, 3 (2018).
3. K.S. Siow, S.T. Chua, and B.D. Beake, *J. Mater. Sci-Mater. Electron.* 30, 6212 (2019).
4. V.R. Manikam and K.Y. Cheong, *IEEE Trans. Compon. Packag. Manuf.* 1, 457 (2011).
5. Q. Xun, B. Xun, Z. Li, P.L. Wang, and Z.D. Cai, *Renew. Sustain. Energy Rev.* 70, 1336 (2017).
6. H.K. Shao, A.P. Wu, Y.D. Bao, Y. Zhao, and G.S. Zou, *Trans. Nonferr. Met. Soc.* 27, 722 (2017).
7. V.C. Nachiappan, J.H. Hattel, and J. Hald, *Microelectron. Eng.* 88, 981 (2011).
8. W.M. Chen, P. Mccloskey, and S.C. O'Mathuna, *Microelectron. Reliab.* 46, 896 (2006).
9. W. Nico, J. Shan, I.D. Liliana, and L. Christian, *J. Mater. Eng. Perform.* 23, 1585 (2014).
10. J. Cho, R. Sheikhi, S. Mallampati, and Y. Liang, in *ECTC Conference Proceedings* (2017), p 1553.
11. G. Wei, G.S. Zou, A.P. Wu, H.L. Bai, and J.L. Ren, *Physica C* 470, 115 (2010).
12. J.N. Calata, T.G. Lei, and G.Q. Lu, *Int. J. Mater. Product Technol.* 34, 95 (2009).
13. A. Sharif, C.L. Gan, and Z. Chen, *J. Alloys Compd.* 587, 365 (2014).
14. F. Yu, H. Liu, C. Hang, and M.Y. Li, *JOM* 71, 3049 (2019).
15. F. Brem, C. Liu and R. Déborah, in *ESTC Conference Proceedings* (2012), p 1.
16. J.F. Li, P.A. Agyakwa, and C.M. Johnson, *Acta Mater.* 59, 1198 (2011).
17. S.W. Yoon, M.D. Glover, and K. Shiozaki, *IEEE Trans. Power Electron.* 28, 2448 (2013).
18. H. Shao, A. Wu, Y. Bao, Y. Zhao, and G. Zou, *J. Mater. Sci-Mater. Electron.* 27, 4839 (2016).
19. T. Shuang, Z. Jian, X. Feng, R. Cao, and F. Wang, *J. Mater. Sci-Mater. Electron.* 29, 16388 (2018).
20. H.Y. Zhao, J.H. Liu, Z.L. Li, X.G. Song, Y.X. Zhao, H.W. Niu, H. Tian, H.J. Dong, and J.C. Feng, *Metall. Mater. Trans. A* 49, 2739 (2018).
21. P. Yao, X.Y. Li, X.B. Liang, B. Yu, F.Y. Jin, and Y. Li, *Mater. Charact.* 131, 49 (2017).
22. J.F. Li, P.A. Agyakwa, and C.M. Johnson, *Acta Mater.* 58, 3429 (2010).
23. A.A. Wronkowska, A. Wronkowski, and K. Kuklinski, *Appl. Surf. Sci.* 256, 4839 (2010).
24. G.T. Lim, B.J. Kim, and K. Lee, *J. Electron. Mater.* 38, 2228 (2009).
25. Y. Tian, C. Hang, X. Zhao, B. Liu, N. Wang, and C. Wang, *J. Mater. Sci-Mater. Electron.* 25, 4170 (2014).
26. J.B. Lee, H.Y. Hwang, and M.W. Rhee, *J. Electron. Mater.* 44, 435 (2015).
27. L. Litynska, J. Wojewoda, P. Zieba, M. Faryna, W. Gust, and E.J. Mittemeijer, *Acta Mater.* 145, 107 (2004).
28. Z. Wu, J. Cai, Q. Wang, J. Wang, and D. Wang, *J. Electron. Mater.* 46, 1 (2017).

Publisher's Note Springer Nature remains neutral with regard to jurisdictional claims in published maps and institutional affiliations.